Received: 14 January 2022 | Revised: 8 April 2022 | Accepted: 14 April 2022

DOI: 10.1002/esp.5389

RESEARCH ARTICLE

ESPL WILEY

# Declassified intelligence satellite imagery as a tool to reconstruct past landforms and surface processes: The submerged riverscape of the Tigris River below the Mosul Dam Lake, Iraq

Luca Forti[1,2] | Guido S. Mariani[3] | Filippo Brandolini[4] | Andrea Pezzotta[1] | Andrea Zerboni[1]

[1]Dipartimento di Scienze della Terra 'A. Desio', Università degli Studi di Milano, Milan, Italy

[2]Istituto di Geoscienze e Georisorse, Consiglio Nazionale delle Ricerche, Pisa, Italy

[3]Dipartimento di Scienze Chimiche e Geologiche, Università degli Studi di Cagliari, Cagliari, Italy

[4]McCord Centre for Landscape – School of History, Classics and Archaeology, Newcastle University, Newcastle upon Tyne, UK

**Correspondence**
Luca Forti, Università degli Studi di Milano, Dipartimento di Scienze della Terra 'A. Desio', Via L. Mangiagalli 34, I-20133 Milan, Italy.
Email: luca.forti@unimi.it

**Funding information**
Università degli Studi di Milano; Ministry of Education, Grant/Award Number: WP4; University of Udine

## Abstract

Located along the Tigris River in the Kurdistan Region of Iraq, the Mosul Dam Reservoir is the second biggest dam of the Near East and represents an important water storage for local human activities. The dam was built between 1981 and 1988 north of the village of Eski Mosul, submerging the course of the Tigris River for c. 100 km. The analysis of historical images derived from declassified Corona satellite imagery acquired between December 1967 and August 1968 reveals the pristine pattern of the Tigris River, including the seasonal changes of its riverbed, shifting across the hydrological year from meandering to anastomosing patterns. Geomorphological mapping based on Corona images allowed us to estimate the seasonal modification of fluvial elements such as the floodplain and point, middle and longitudinal bars. The comparison with Landsat data collected since the 1990s showed the first phases of the basin filling and the control on the present-day aspect of the lake inherited from the setting of the Tigris channel belt and, more in general, the litho-structural control over the evolution of the local hydrographic network; we also document the influence of the original Tigris River course on its recent insertion into the lake. Our work allowed reconstruction of the ancient fluvial landscape below the Mosul Dam Lake and the evolution of its riverscape controlled by litho-structural factors and seasonal variations of the river discharge. Finally, this contribution highlights the relevance of declassified intelligence satellite imagery in interpreting natural geomorphic processes and landforms, today altered by human agency.

**KEYWORDS**
fluvial geomorphology, Iraq, Mosul Dam Lake, riverscape, seasonality, Tigris River

## 1 | INTRODUCTION

Rivers are among the most dynamic environments in terms of landscape change and impact on human communities (Buffington & Montgomery, 2013; Charlton, 2007; Dollar, 2004; Jézéquel et al., 2022; Tadaki et al., 2014; Thorndycraft et al., 2008). Their evolution depends on numerous factors, ranging from tectonics and climate to human intervention, often difficult to recognize as separate triggers and in many cases deeply modified by recent human agency (Brown et al., 2017; Tarolli et al., 2019). Remote sensing and field investigations on water courses and their surrounding landscapes can help in the reconstruction of the processes underlying fluvial evolution. This is especially true for arid regions, where the poor plant cover allows very precise and detailed observations, even from remote locations (Perego et al., 2011). Moreover, in such contexts the effects of lithological and structural constraints are more immediate to be identified

(Zerboni et al., 2020), greatly helping the formulation of more effective models.

Among the great rivers of the planet, the Tigris and the Euphrates are very important for the natural and human history of Mesopotamia, in the past as well as today. Their courses, from Turkey to the Gulf, are controlled for the most part by the structural evolution of the region, a quite active area of converging plates (Al-Dabbagh & Al-Naqib, 2009; Al-Saigh, 2008; Fouad, 2012; Sissakian et al., 2020). The Tigris River flows for 1800 km from the Taurus mountains in Turkey through the border with Iraq and then into the Gulf. Almost 56% of its basin lies in Iraq, with six major tributaries and secondary rivers draining most of the runoff from the Iraqi mountainside of the southern Zagros. The Tigris River is less meandering than the Euphrates, and along many of its branches, especially after the Iraq–Turkey border, its course is strongly influenced by the geodynamic setting of the Arabian–Eurasian plate convergence. In modern times, the course of the Tigris River has been constrained in multiple places by human action through the construction of dams, which greatly modified the local landscape and flooded several villages and archaeological sites (ESCWA, 2013; Sconzo & Simi, 2020; Titolo, 2021). At the same time, new artificial basins show non-homogeneous aspects, which probably follow previous natural constraints, ultimately related to the settings of the ancient course of the Tigris River. In the contexts of artificial lakes, despite the arid climate and the low plant cover allowing very good visibility of ground features, it is hard to map landforms and interpret the factors triggering the evolution of fluvial landforms since a relevant portion of the landscape is submerged and invisible to field observation.

To overcome this issue, in the present work we combine geological and geomorphological data with the observations of declassified satellite images collected before the construction of the Mosul Dam, thus representative of the pristine local riverscape. Such a multitemporal mapping approach (Zerboni et al., 2020) aims to: (i) reconstruct the ancient course of the Tigris River upstream of Mosul; (ii) describe its seasonal dynamics before the construction of the dam; and (iii) correlate the current dynamic of the lake to lithological and structural factors that in the past may have controlled the development of the river. The use of a multidisciplinary approach permitted us to reconstruct the submerged riverscape of the Tigris River, showing the underlying causes that shaped fluvial dynamics as much as the current lake and helping in the reconstruction of past geomorphic processes. Finally, we highlight the relevance of declassified intelligence satellite imagery as a tool to interpret the dynamics of past geomorphic processes and landforms today, influenced/altered/obscured by human agency.

## 2 | STUDY AREA

### 2.1 | Geological and climatic background

The study area covers 1250 km$^2$ of the northwestern Kurdistan Region of Iraq (KRI) in the governorates of Dohuk and Nineveh (Figure 1). The landscape is the result of the interplay between geological–structural, geomorphological and climate-driven processes

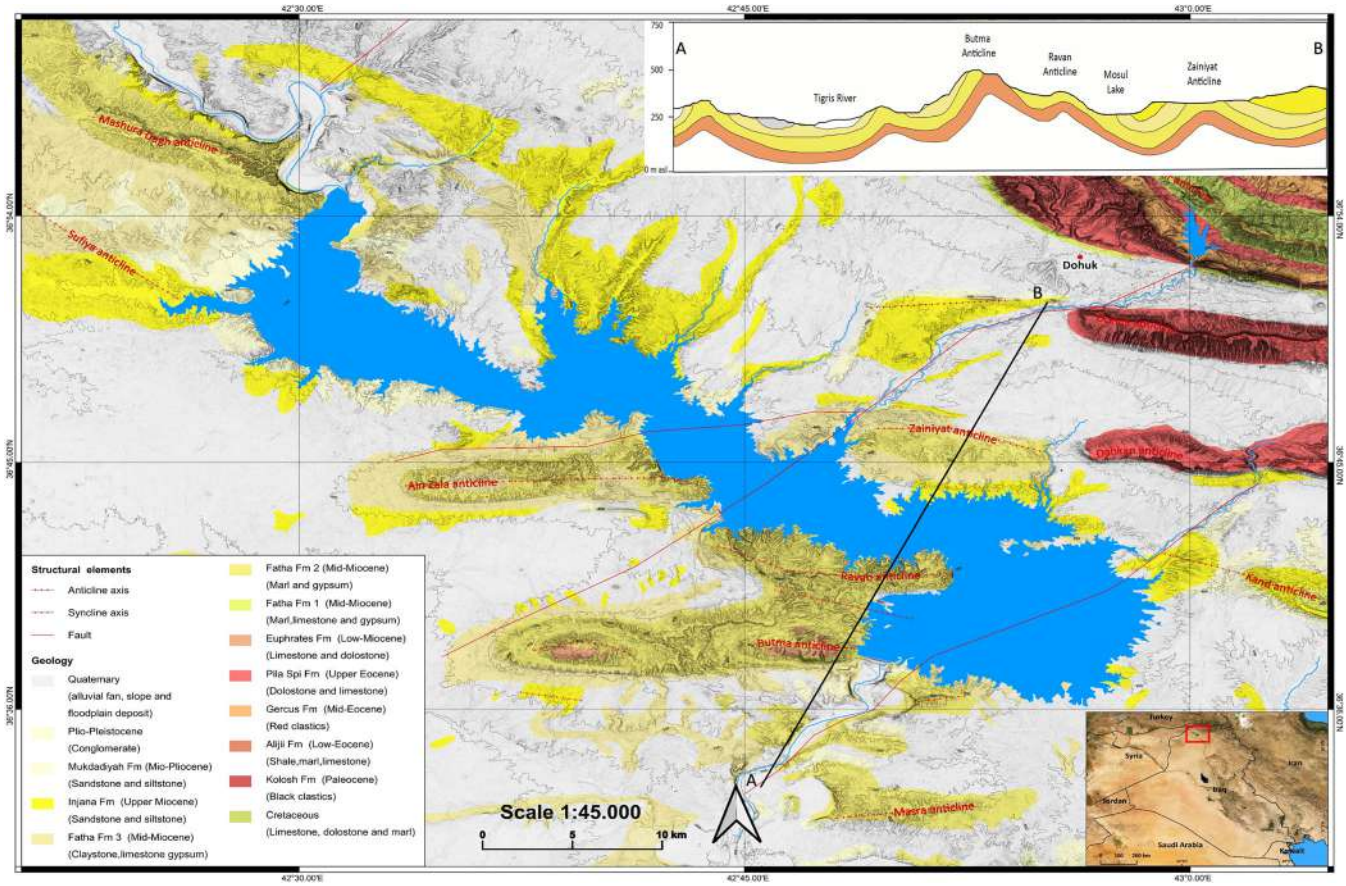


**FIGURE 1** Simplified geological map and main structural elements of the study area (elaborated from Al-Mosul quadrangle geological map of the Ministry of Industry and Minerals, Iraq Geological Survey, 1995, 1997, 2014). The black line indicates the trace of the geological cross-section showing the local anticline and syncline systems.

(Forti et al., 2021), and subsequently the construction of the dam and its infilling in the 1980s (Adamo & Al-Ansari, 2016).

The area is in the Low Folded Zone, within the Outer Platform of the Arabian Plate part of the Zagros-Fold Thrust Belt (ZFTB; Fouad, 2007). This structure is the result of the collision between the Arabian and Eurasian continental plates that started in the Early Miocene and is still actively progressing today (Csontos et al., 2012; Dercourt et al., 1986; Fouad, 2012; Mouthereau et al., 2012). Low-elevation mountains and lowlands characterize the area. Their distribution is controlled by the presence of anticline ridges, mainly oriented W–E (Ain Zala, Zainiyat, Butma, Ravan, Dohuk, Dakhan, Masra and Kand anticline) (Figures 1, 2a and b) and NW–SE (Mashura Dag, Sufiya and Baikhair) (Abdulnaby, 2019; Fouad, 2012) and by the NW–SE development of the Dohuk Fault System (sensu Al-Dabbagh & Al-Naqib, 2009; Al-Saigh, 2008, 2012) with the main alignment of the Sasa-Bekhair Fault (Fouad, 2012; Sissakian et al., 2018).

The anticline ridges are mainly composed of Paleocene to Lower Miocene limestone and dolostone, whereby in the Mosul Lake area the anticline is characterized by the Miocene to Mio-Pliocene Fatha, Injana and Mukdadiyah formations, alternating marl and gypsum with sandstone and limestone (Sissakian & Fouad, 2012) (Figures 1, 2d). Plio-Pleistocene conglomerates outcrop along the northern banks of Mosul Lake and in the proximity of the dam (Figure 2c) (Al-Dabbagh & Al-Naqib, 1991; Sissakian & Al-Jibouri, 2012).

Quaternary deposits are mainly located along the hillslopes of anticlines and in the lowland areas of the syncline troughs. They include fluvial, floodplain, alluvial fan, colluvial and anthropogenic deposits (Forti et al., 2021; Jassim & Goff, 2006; Sissakian & Al-Jibouri, 2012). Quaternary deposits are composed of conglomerates with fine to coarse sand, with levels of silt and clay recognized at different locations of the area, especially on the fluvial terraces above the banks of the Tigris River (Al-Dabbagh & Al-Naqib, 1991). Such deposits are eroded and reworked by the action of the fluvial network draining from the northeast into the Mosul Lake to the southwest.

Climatic data for the study area derive from a meteorological station placed in the cities of Mosul and Dohuk and were elaborated for climate models by Awchi and Kalyana (2017) and Sulaiman (2016). Models suggest that the Mosul Lake is located between two climatic zones of the climate classification proposed by Koppen and Geiger (1936). The first zone is the Mediterranean or Dry Summer Subtropical (Csa), while the second one is the Subtropical Steppe (Bsh) (Malinowski, 2002; Salman et al., 2019). The Csa climatic zone in this area is characterized by extremely to moderately cold wet winters and moderately hot arid summers. Precipitations occur during the winter and spring seasons from November to April, with an estimated mean rainfall at Dohuk station of 570 mm and seasonal temperature variations from 8.8 to 34°C (Awchi & Kalyana, 2017; Malinowski, 2002; Sulaiman, 2016). The Bsh climate zone has moderately cold winters and hot to extremely hot dry summers. Long-term climate data extrapolated from the Mosul meteorological station (Awchi & Kalyana, 2017) show that most rainfall occurs during the winter season and the annual mean rainfall from 1937 to 2010 is 378 mm. Annual mean temperature is 21°C, with extremely hot summers with mean temperatures of around 40°C.

Most rivers in the region are ephemeral, active during the rainy season (Othman & Gloaguen, 2013) and inactive in the dry season; only the Tigris River and a few of its tributaries are perennial. Several climate models showed a strong increase of drought events in recent times. From the 1980s to the 1990s, the area surrounding the Mosul Lake suffered several periods of drought. At the beginning of the 1990s and especially in the last decades of the 20th century, severe droughts are recorded (Al-Khafaji & Al-Ameri, 2021; Alwan

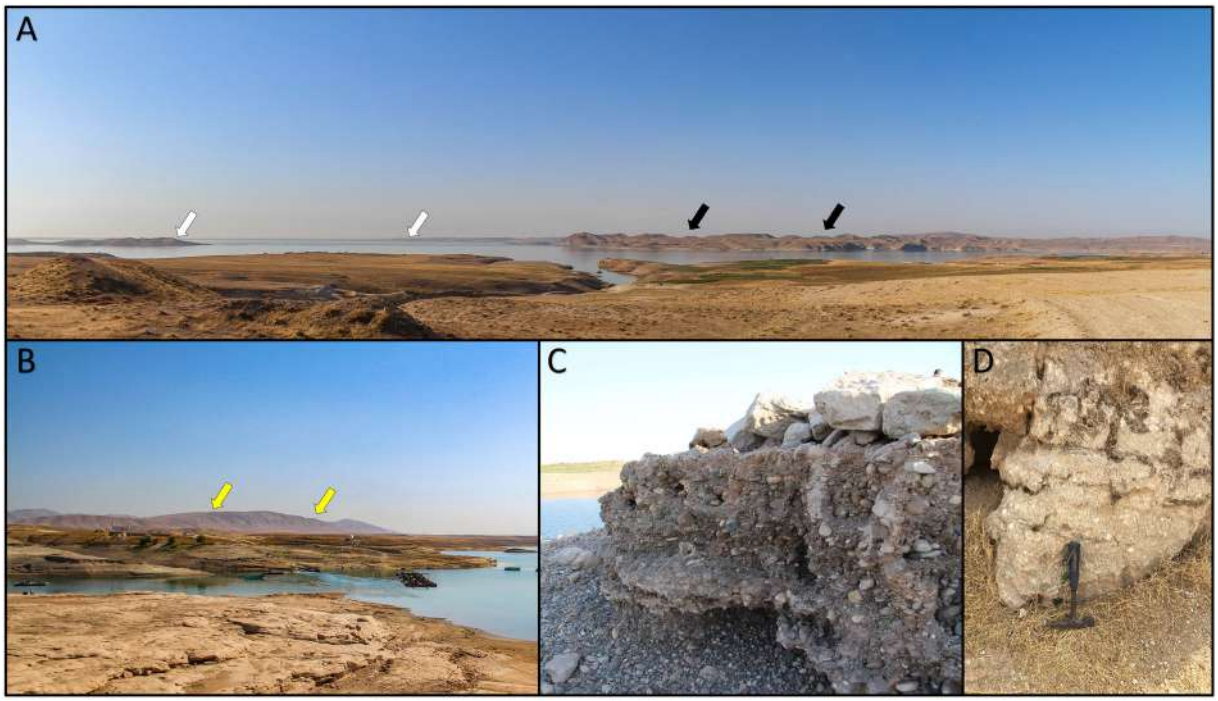


**FIGURE 2** Field pictures from the MDL area. (A) Panoramic view from the left bank of MDL at a high stand in 2015; on the background the ridge of the Ravan anticline (black arrows) and the area of the dam (white arrows). (B) Panoramic view from the left bank of MDL towards the east; on the background the ridge of the Dakhan anticline (yellow arrows). (C) An outcrop of the Plio- Pleistocene conglomerates close to the left bank of MDL. (D) An outcrop of the gypsum-rich layers of Fathma Formation

et al., 2019; Awchi & Kalyana, 2017). In addition to climate change, the dam's water supply has been threatened by ongoing conflicts in the area over the past four decades (Hasan et al., 2019).

## 2.2 | Hydrological setting of the Tigris River and the Mosul Dam Lake

The Tigris River originates in Turkey along the southern slope of the Taurus mountains (Altinbilek, 2004). The river flows through Turkey, Syria and Iraq. After 1800 km the Tigris River merges with the Euphrates River in the South of Mesopotamia, forming the Shatt-Al-Arab River that flows into the Gulf, 220 km downstream (Figure 3a).

The main tributaries from Iraq and Syria are the Feysh Khabur, Great Zab, Lesser Zab, Adhaim and Diyala rivers. The Feysh Khabur River joins the Tigris River west of the municipality of Zacko, while the Great Zab and Lesser Zab rivers, respectively, to the southeast of the cities of Mosul and Fatha. The Adhaim and Diyala rivers merge into the Tigris River south of Fatha and in the proximity of Baghdad; afterwards, no major tributary rivers are recognized except for a few agricultural canals draining from the Zagros piedmont in the internal floodplain of the Tigris River. The Tigris River drainage basin occupies a total area of ~221 000 km$^2$ for the 60% in Iraq territory; its mean discharge at Mosul city was 700 m$^3$/s in 1984 and dropped to 596 m$^3$/s after the construction of the dam. The overall amount of the Iraqi catchment area is ~124 000 km$^2$; the annual mean discharge changes according to the Tigris setting and the minor tributary basins to the south (Figures 3b and c) (Al-Ansari, 2013; Al-Ansari & Knutsson, 2011; ESCWA, 2013; Saleh, 2010).

The MD is the largest dam in Iraq and one of the biggest in the Near East, with a storage capacity of 11.11 km$^3$ of water (Adamo & Al-Ansari, 2016). It is 3650 m in length and 113 m high, with an embankment core composed of clays. It was built to provide water for irrigation, control floods and generate hydropower (Figure 4). During the preparation of the site for construction operations, problems related to grouting work on the foundations of the dam were recognized (Adamo et al., 2015, 2019). In fact, the geological bedrock of the dam consists of gypsum, marl and limestone layers, interbedded with breccias, which are intensely fractured by the Dohuk Fault System, allowing seepage and karst processes to act on the stability of the dam (Al-Dabbagh & Al-Naqib, 2009; Al-Saigh, 2008, 2012; Sissakian et al., 2014). Construction work started in January 1981 and the dam became operational in July 1986.

# 3 | MATERIALS AND METHODS

To investigate the recent evolution of the Tigris River and its riverscape in the area submerged by the Mosul Dam Lake (MDL), including the major factors controlling its development, we performed a detailed geomorphological mapping of the area and an analysis of its seasonal changes.

Geomorphological mapping of the area was performed on data interpreted from both declassified Corona, Landsat, Sentinel-2A/B, Esri World Imagery, Bing Virtual Earth and GoogleEarth™ satellite images (Bing Maps, 2021; Esri, 2021) (Figure 5). The declassified Corona satellite image dataset was downloaded from the CAST Atlas of the University of Arkansas (https://cast.uark.edu/research/corona.php) (USGS, 1968); in particular, we considered December 1967 (1102–1025) and August 1968 (1104–2138) images. Landsat and Sentinel-2 images were selected from the EarthExplorer platform of the USGS (https://earthexplorer.usgs.gov) and cover a period from June 1984 to August 1986 and March and July 2016–2020. We used 11 declassified Corona, 15 Landsat and 11 Sentinel-2 images (Table 1). Landsat and Sentinel-2 imagery was observed in false colours (red = band 4, green = band 3, blue = band 2). Corona imagery was observed in single-band greyscale.

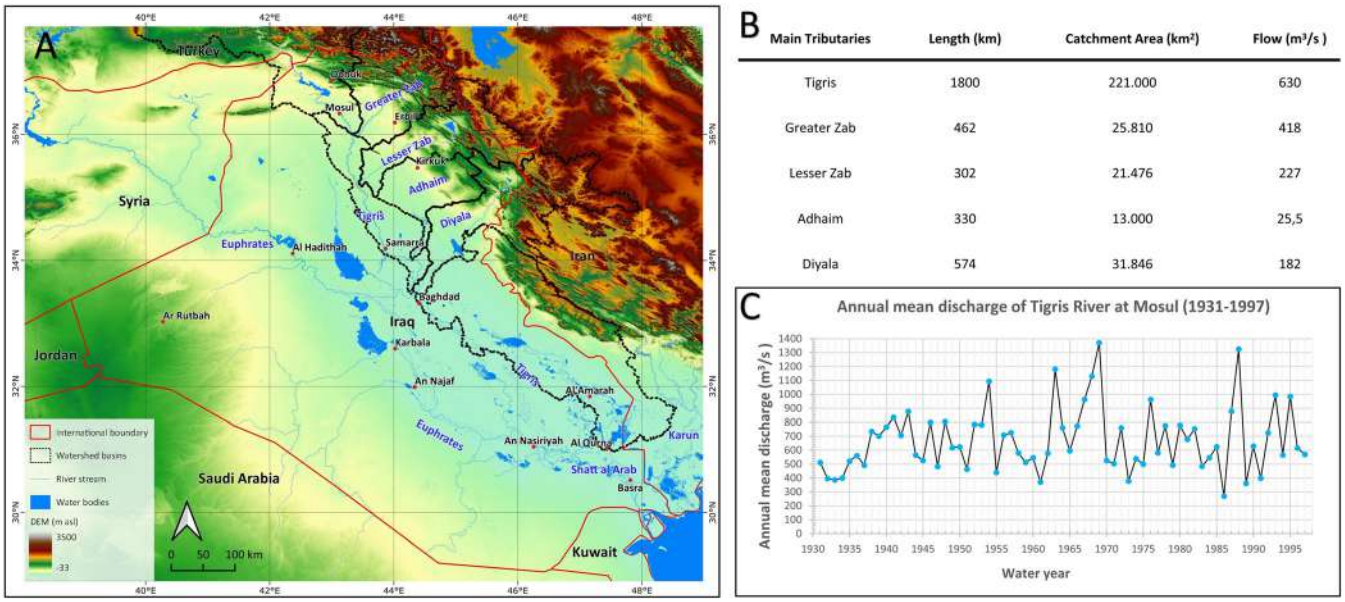


**FIGURE 3** (A) Iraqi watershed basin of the Tigris River and its main tributaries extrapolated and superimposed on a MERIT DEM. (B) Information about length, catchment area and mean flow of the Tigris River and its major tributaries (Al-Ansari, 2013; Al-Ansari & Knutsson, 2011; ESCWA, 2013). (C) Annual mean discharge of the Tigris River at the Mosul stream gauge derived from the USGS database (Saleh, 2010)

**FIGURE 4** Bing Virtual Earth imagery of Mosul Dam site; notice the dam operation and the huge anthropogenic impact on the surrounding landscape

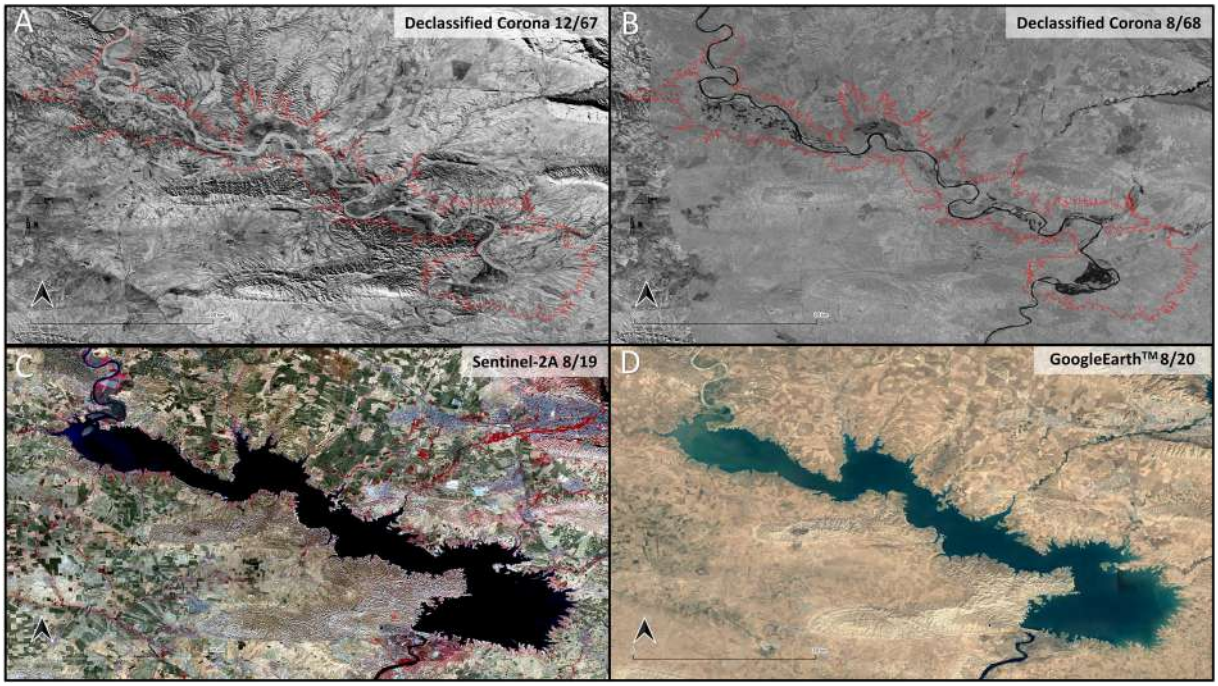


**FIGURE 5** (A, B) Declassified Corona satellite images of the ancient Tigris riverscape below the MDL taken in two different phases of discharge. The red line is the current size of the MDL. (C, D) The current shape of the MDL elaborated from Sentinel-2A (false colours) and Google Earth™

Corona images helped in mapping landforms to understand their seasonal geomorphic shift (Gilvear & Bryant, 2016; Gurnell et al., 2003). The mapping considered different geomorphic units, illustrating the effect of fluvial, slope and anthropogenic processes. Fluvial geomorphic units are the most important for our study and were described to highlight seasonal changes in the fluvial pattern; we adopted the classification proposed by Brierley and Fryirs (2013). Landsat images taken from 1984 to 1986 were used to emphasize the time and steps of the infilling of the MDL. Moreover, true-colour GoogleEarth™, Bing Virtual Earth and Esri World Imagery images were used to investigate the influence of the ancient river planform of the Tigris River on the present setting of the Mosul Lake. The choice of specific dates for Sentinel-2A/B imagery is based on known operations and discharge variations for 2016, 2019 and 2020, as they were used for detecting seasonal fluctuations of lake shorelines controlled by variations in the discharge of the Tigris and seasonal dam

**TABLE 1** Database of satellite imagery used in this work; the monthly discharge of the Tigris River is reported when available

| Dataset | Name | Period | Ground resolution | Monthly mean discharge ($m^3/s$) (MOS) |
|---|---|---|---|---|
| Decassified Corona Image | ds1102-1025df006 | 12/11/1967 | 6 ft | 481.4 |
| Decassified Corona Image | ds1102-1025df007 | 12/11/1967 | 6 ft | |
| Decassified Corona Image | ds1102-1025df008 | 12/11/1967 | 6 ft | |
| Decassified Corona Image | ds1102-1025df010 | 12/11/1967 | 6 ft | |
| Decassified Corona Image | ds1102-1025df015 | 12/11/1967 | 6 ft | |
| Decassified Corona Image | ds1102-1025df016 | 12/11/1967 | 6 ft | |
| Decassified Corona Image | ds1104-2138da003 | 8/16/1968 | 6 ft | 211.6 |
| Decassified Corona Image | ds1104-2138da004 | 8/16/1968 | 6 ft | |
| Decassified Corona Image | ds1104-2138da005 | 8/16/1968 | 6 ft | |
| Decassified Corona Image | ds1104-2138da006 | 8/16/1968 | 6 ft | |
| Decassified Corona Image | ds1104-2138da007 | 8/16/1968 | 6 ft | |
| Landsat 4–5 Thematic Mapper | LT05_L1TP_170034_19840606 | 6/6/1984 | 30 m | 535.4 |
| Landsat 4–5 Thematic Mapper | LT05_L1TP_170035_19840606 | 6/6/1984 | 30 m | |
| Landsat 4–5 Thematic Mapper | LT05_L1TP_170034_19840926 | 9/26/1984 | 30 m | 118 |
| Landsat 4–5 Thematic Mapper | LT05_L1TP_170035_19840926 | 9/26/1984 | 30 m | |
| Landsat 4–5 Thematic Mapper | LT05_L1TP_170034_19841012 | 10/12/1984 | 30 m | 191.1 |
| Landsat 4–5 Thematic Mapper | LT05_L1TP_170035_19841231 | 12/13/1984 | 30 m | 659.3 |
| Landsat 4–5 Thematic Mapper | LT05_L1TP_170034_19850116 | 1/16/1985 | 30 m | 350.6 |
| Landsat 4–5 Thematic Mapper | LT05_L1TP_170035_19850116 | 1/16/1985 | 30 m | |
| Landsat 4–5 Thematic Mapper | LT05_L1GS_170034_19860103 | 1/3/1986 | 30 m | 92.1 |
| Landsat 4–5 Thematic Mapper | LT05_L1GS_170035_19860103 | 1/3/1986 | 30 m | |
| Landsat 4–5 Thematic Mapper | LT05_L1TP_170034_19860220 | 2/20/1986 | 30 m | 102.5 |
| Landsat 4–5 Thematic Mapper | LT05_L1TP_170035_19860220 | 2/20/1986 | 30 m | |

(Continues)

**TABLE 1** (Continued)

| Dataset | Name | Period | Ground resolution | Monthly mean discharge ($m^3/s$) (MOS) |
|---|---|---|---|---|
| Landsat 4–5 Thematic Mapper | LT05_L1TP_170034_19860815 | 5/15/1986 | 30 m | 553.5 |
| Landsat 4–5 Thematic Mapper | LT05_L1TP_170034_19860628 | 6/28/1986 | 30 m | 503.1 |
| Landsat 4–5 Thematic Mapper | LT05_L1TP_170035_19860628 | 6/28/1986 | 30 m | |
| Landsat 4–5 Thematic Mapper | LT05_L1TP_170035_19860815 | 8/15/1986 | 30 m | 296.5 |
| Sentinel-2 | S2A_OPER_MSI_L1C_TL_MTI__20160308T080055_20160308T115917_A003707_T38SKF_N02_01_01 | 3/8/2016 | 10 m | |
| Sentinel-2 | S2A_OPER_MSI_L1C_TL_MTI__20160308T080055_20160308T115917_A003707_T38SLF_N02_01_01 | 3/8/2016 | 10 m | |
| Sentinel-2 | L1C_T38SKF_A005709_20160726T075850 | 7/26/2016 | 10 m | |
| Sentinel-2 | L1C_T38SLF_A005709_20160726T075850 | 7/26/2016 | 10 m | |
| Sentinel-2 | S2B_MSIL2A_20191106T080029_N0213_R035_T38SKF | 8/11/2019 | 10 m | |
| Sentinel-2 | S2A_MSIL2A_20191108T075131_N0213_R135_T38SLF_ | 8/11/2019 | 10 m | |
| Sentinel-2 | L1C_T38SKF_A024628_20200310T080339 | 3/10/2020 | 10 m | |
| Sentinel-2 | L1C_T38SLF_A024628_20200310T080339 | 3/10/2020 | 10 m | |
| Sentinel-2 | L1C_T37SGA_A026344_20200708T080203 | 7/8/2020 | 10 m | |
| Sentinel-2 | L1C_T37SGA_A026344_20200708T080203 | 7/8/2020 | 10 m | |
| Sentinel-2 | L1C_T38SLF_A026301_20200705T075705 | 7/8/2020 | 10 m | |

operations. We reconstructed the discharge for the Tigris River c. 20 years before the start of the construction of the dam, namely for the period between December 1967 and August 1968 (declassified Corona satellite imagery). The same was done for the period between 1984 and 1986, during the filling steps of the basin (Landsat imagery).

Remote-sensed images were projected in the UTM Zone 38 reference system and used as the background for remote observations in QGIS 3.16 software. Also, digital elevation model (DEM) MERIT with 3 arcsec horizontal resolution (~90 m at the equator) was projected in the UTM Zone 38 and used to extrapolate the Tigris and tributaries watershed (Yamazaki et al., 2017). The geological bedrock and main linear structural features were extracted from the Al-Mosul Quadrangle geological map (1:250 000) of the Geological Map Series of Iraq and from the Tectonic Map of Iraq (Fouad, 2012); additional structural data come from Al-Dabbagh & Al-Naqib (2009), Al-Saigh (2008) and Sissakian et al. (2018).

## 4 | RESULTS

### 4.1 | Geomorphological variability of the Tigris riverscape before the Mosul Dam Lake

The comparison between declassified Corona imagery from December 1967 and 1968 revealed several changes in the river planform, including variations in the setting of mid-channel and bank-attached landforms. In response to the seasonal variation of discharge (meant as flow stage), the behaviour of the river, or at least some of its parts, starts to adjust and re-equilibrate erosional and depositional processes (Figure 5).

The relationship between discharge variations and river pattern is strongly connected with the lithological and structural setting in which the Tigris River flows. In the study area, the Tigris River changes between different structural settings, which are ultimately related to the effects of the evolution of the local anticline–syncline system and the Dohuk Fault System. In fact, the anticline–syncline system influenced the ability of the river to cut into the bedrock and thus the width of its valley. Consequently, the Tigris River below the MDL shifts from partly confined to unconfined and the river planform is not homogeneous. Also, these elements impact on the shape and width of the floodplain and its related geomorphic units.

### 4.2 | Geomorphological mapping of the winter season

The declassified Corona imagery taken on 11 December 1967 recorded the Tigris River at its bankfull stage. At that time, the monthly mean discharge at the streamflow gauging station of Mosul was 481.40 $m^3/s$. The main recognizable features are fluvial landforms related to the active channel stream point and the mid-longitudinal bars. On the banks of the active channel a sequence of three levels of terraces is visible (T1, T2 and T3, oldest to youngest) (Figure 2c). Some reach banks of the Tigris River show an erosional

scarp caused by undercutting and gravity collapse. Floodplains are in the proximity of the sinuous reach of the Tigris River; most of them display active chute channels and meander scars with traces of paleochannels. The latter were exploited for cultivation. Moreover, secondary tributaries are mainly distributed along the left bank of the Tigris; they flow along the erosional pediment that connects the anticline slope to the river (Figure 6).

The lithological and structural setting of the bedrock affected the morphodynamics of the Tigris River, but also influenced the other geomorphological processes acting in its proximity. A homogeneous belt of flatirons is visible on anticline hills; minor streams also dissect the hillsides creating badlands upon marls, gypsum and conglomerate outcrops.

South of the dam site, a landslide body and its denudation surface occur; the curved geometry of the foot of the deposit modifies the course of the Tigris River, forcing the development of an irregular meander.

### 4.3 | Geomorphological mapping of the summer season

The declassified Corona images taken on 16 August 1968 capture the Tigris River during a low-flow stage. The monthly mean discharge recorded at the streamflow gauging station of Mosul was 211.60 $m^3/s$. Compared with the winter season, the general landscape of the area does not show evident changes. On the other hand, within and along the main course of the Tigris River visible variations appear. The low water level exposes several mid-channel and bank-attached geomorphic features, which reflect the variety of landforms—and related processes—that changed during the seasonal fluctuation of discharge (Figure 7).

The main mid-channel geomorphic units recognized relate to the width of the channel and to the type and shape of the planform in which they developed. In the northern part of the map, the river shows a decrease in the number of channels in which it flows. A single channel with low sinuosity and few meanders shifts to a course with multiple meanders and up to three channels. In general, compound and point bars occur on the convex banks of tortuous meander bends (Figure 8a). Bars are covered by ephemeral vegetation, with slack water confined in chute channels and in the scours. Downstream, asymmetrical lateral bar, scroll bars and mainly mid-channel bar units form along the low-sinuosity reach (Figures 8b and c). The mid-channel units are composed of raindrop-shaped longitudinal bars, elongated along the direction of the flow, and diagonal bars, oval to sigmoidal in shape and oriented perpendicular to the channel banks (Brierley & Fryirs, 2013) (Figures 8d and e). Vegetated mid-channel islands are strictly connected to the channel dynamics, reflecting the river storage capacity for sediments (Brierley & Fryirs, 2013) (Figure 8e). This is, in turn, related to how processes reshaped the river course before and after flood events: in fact, during its low-flow stage the Tigris River displays a multiple channels pattern only where mid-channel islands and compound bars occurred (Figure 8f).

### 4.4 | Factors controlling the Tigris riverbed landscape

Reconstructing the landscape of the Tigris River before the filling of the Mosul Dam Reservoir revealed the main factors that influenced the pattern and planform of channels over time. The different effects of lithology, geological structure and river behaviour allow us to divide the area into three zones: upstream, middle stream and downstream. These are treated separately to better expose the influence of each factor on the diversity of channel shapes.

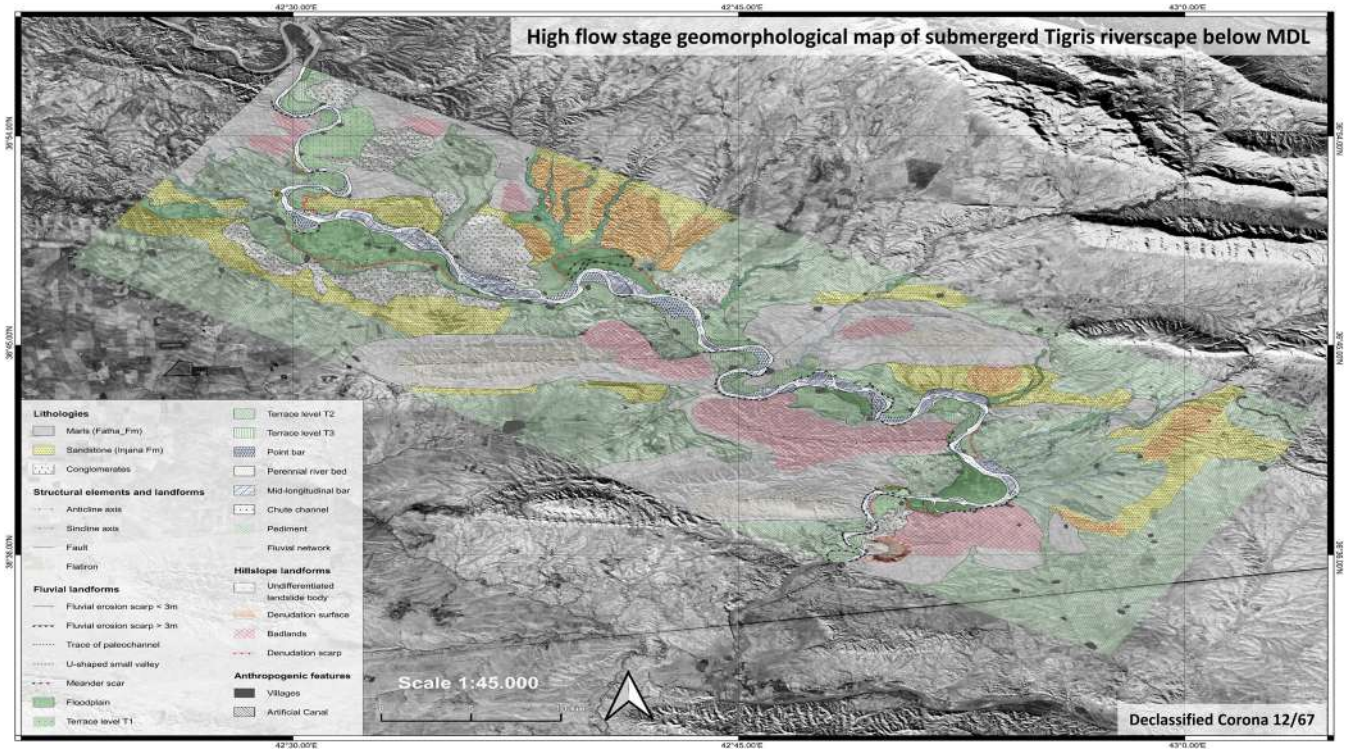


**FIGURE 6** Geomorphological map of the ancient Tigris riverscape elaborated on the declassified Corona satellite image during its high-flow stage (December 1968)

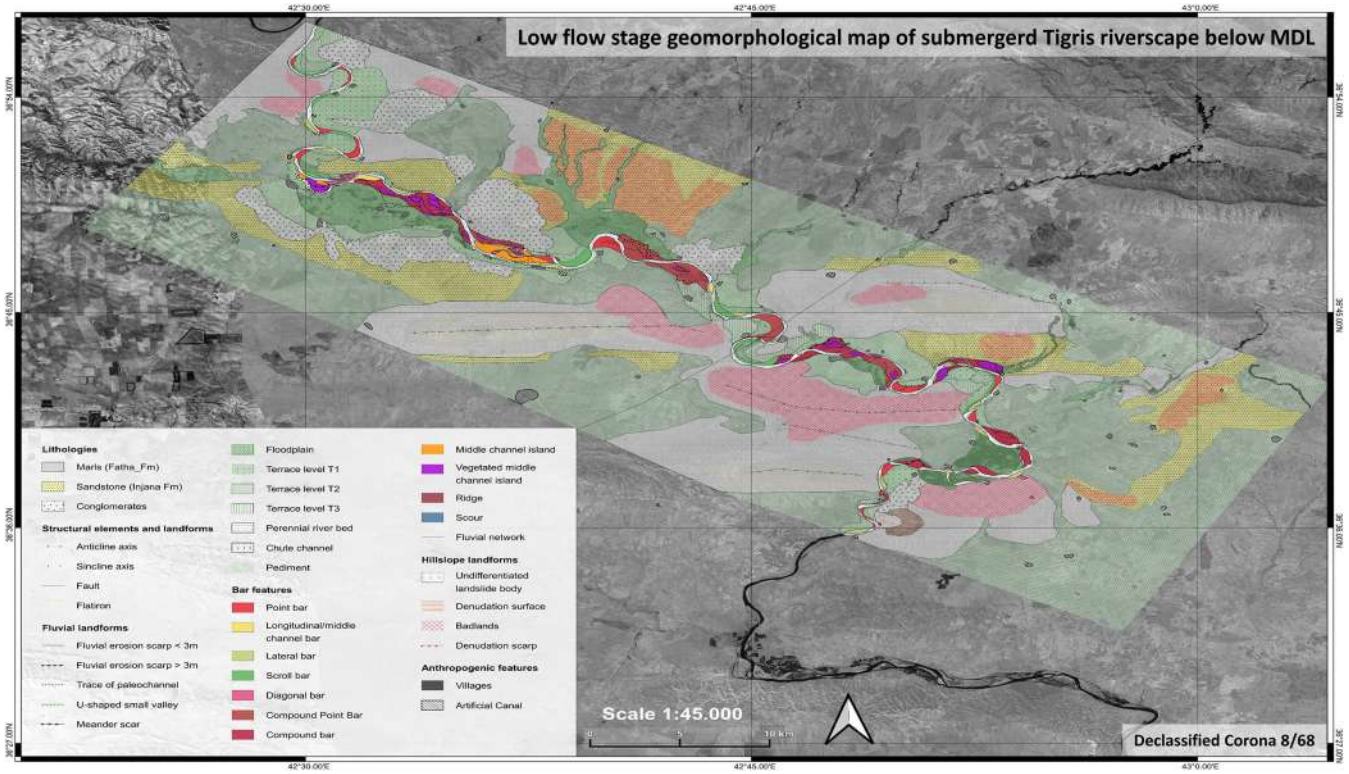


**FIGURE 7** Geomorphological map of the ancient Tigris riverscape elaborated on the declassified Corona satellite image during its low-flow stage (August 1967)

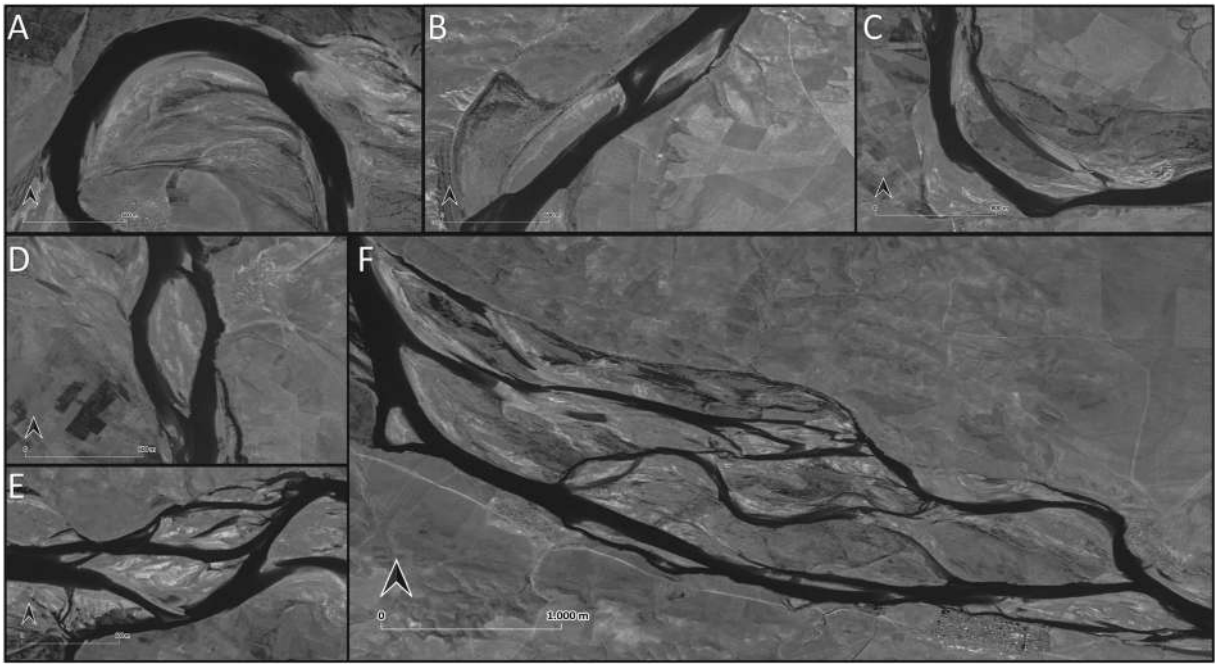


**FIGURE 8** Examples of fluvial bars exposed during low-flow stage derived from declassified Corona acquired in August 1967: (A) point bar; (B, C) lateral and scroll bar; (D, E) longitudinal and diagonal bar; (F) plant-covered mid-channel islands

### 4.4.1 | Upstream lithological controls

The upstream river planform of the Tigris River is c. 43 km long and different river planforms are visible during the bankfull (1967) and low-flow stages (1968) (Figure 9a). The Tigris River changes its sinuosity NW–SE. The first portion of the stream is characterized by tortuous meanders with small point bars and two/three terrace levels; a small floodplain pocket can also sometimes develop when the river course is partly confined inside a narrow valley. Afterwards, the number of channels increases, and the river setting shifts from a wandering to an anabranching gravel bed according to the flow stage (Figures 9b and c). A wide floodplain with meander scars, chute

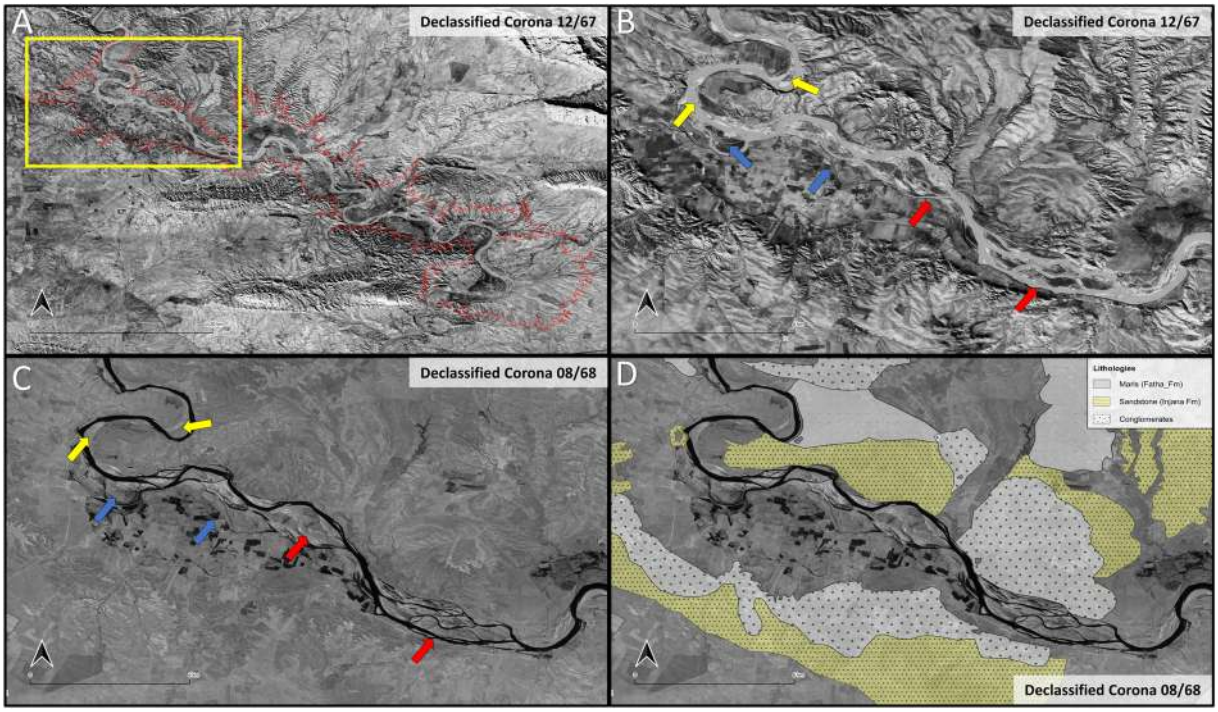


**FIGURE 9** Details from the upstream sector of the river. (A) Position of the area along the Tigris River. Examples from the (B) winter and (C) summer season of the Tigris riverbed; along the northwestern part appear tortuous meanders with small point bars (yellow arrows); then, the number of channels increases, and according to flow stage this sector shifts from wandering to anabranching with gravel bed (red arrows). The right bank hosts a large floodplain with several small fluvial features (blue arrows). (D) Lithological map of this part of the Tigris River catchment highlighting the main rock formations

channels, paleochannels and superimposed agricultural fields characterizes the right bank. On the 1967 Corona image, this part of the river shows a pathway of flood channels active during high-discharge events. The shape of mid-channel and bank-attached geomorphic units varies in both 1967 and 1968. In this portion, the major constraint on the Tigris River dynamic is the lithological change of the bedrock from the marls and sandstones of the Injana and Fatha formations to the Plio-Pleistocene conglomerates (Figure 9d). The latter increases the size of the bed material with coarse-grained sand and pebbles. These materials form river islands, flooded during high-discharge flows and exposed and covered by vegetation in the low-flow stage. The island plant cover ensures the stability of each bar: while the action of erosional and depositional processes can modify their shape with time, they never shift from their original location.

### 4.4.2 | Middle-stream channel shape change

The middle stream is 45 km long and is characterized by a decrease of the braiding degree and a corresponding increase in sinuosity of the channel planform (Figure 10a). The uppermost part of this section follows a meandering pattern, with point bars migrating northwards. More downstream, the low-sinuosity reach hosts a small-pocket floodplain with bank-attached and mid-channel geomorphic features such as longitudinal, lateral and compound bars. Afterwards, two tortuous meanders develop in a confined to partly confined valley; here are visible a compound point bar and an encased convex bend with a scroll bar in the concave zone. In the lowest portion, the river planform changes into an irregular straight planform with lateral bars in the bankfull stage attached at the riverbanks during the low-flow stage (Figures 10b and c). The evolution of this part of the river was influenced by the structure of the anticline ridges of Ain Zala, Ravan and Zainaiyat and by the effects of Dohuk Fault System, driving the development of encased meanders into the marl bedrock of the Fatha Formation (Figure 10d).

### 4.4.3 | Downstream and dam-site diversity

The downstream portion of the Tigris River occupies the last 20 km before the dam site. The river follows a tortuous planform flowing in a partly confined valley setting; wide floodplains form in the inner bend of two meanders and along the left bank of the last straight part of the river before the dam site (Figure 11a). At the low-flow stage, lateral bars and compound bars with point bars occur. A series of flood channels and a wide floodplain occupied by cultivations is visible in the inner part of the point bar, located in the last meander. The floodplain before the dam site is crossed by secondary little branches of the Tigris. During bankfull flow stage, such geomorphic features are submerged and affected by erosional and depositional processes which change their shape and dimensions (Figures 11b and c).

### 4.4.4 | Examples of variations of riverbed and mid-channel to bank-attached geomorphic features

The comparison between declassified Corona images reveals differences in the behaviour of the Tigris River planform and its related

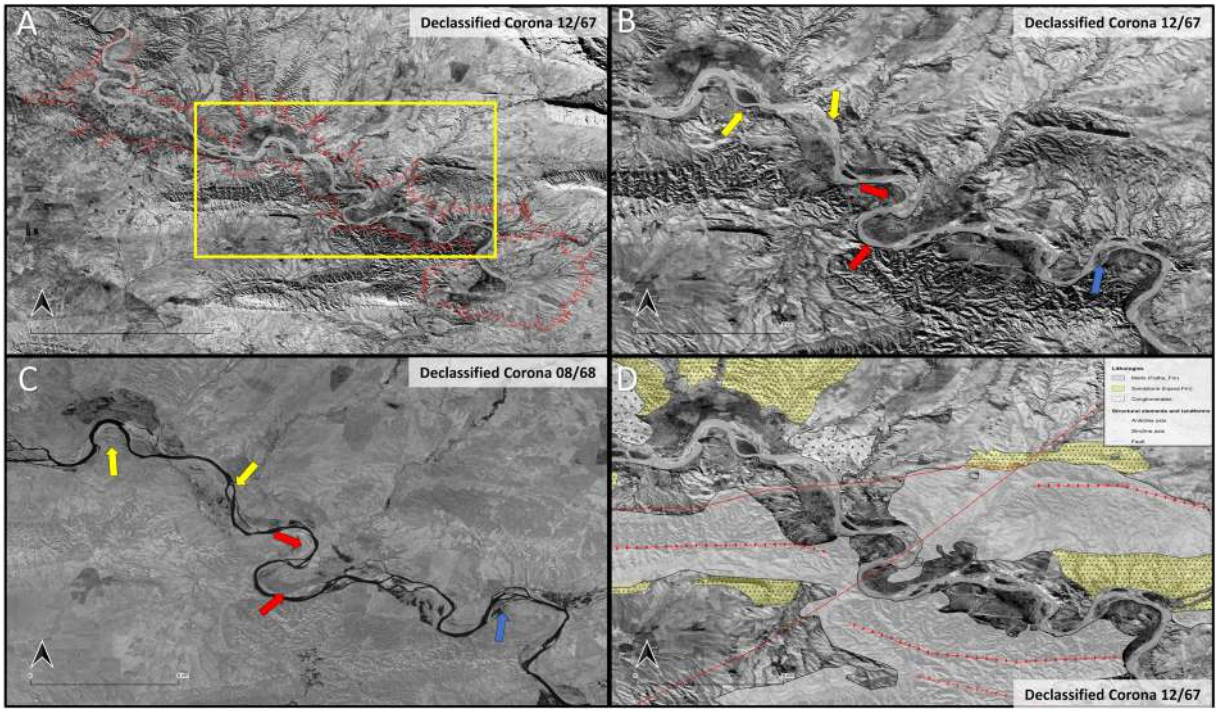


**FIGURE 10** Details from the middle-stream sector of the river. (A) Position of the area along the Tigris River. Examples from the (B) winter and (C) summer season of the Tigris riverbed showing a low sinuosity with longitudinal, lateral and compound bars (yellow arrows). Afterwards, two tortuous meanders develop a point bar in the convex bend and a scroll bar in the concave zone (red arrows). In the lowest portion of the area, the river changes into an irregular straight planform with lateral bars (blue arrow). (D) Lithological and structural map of this part of the Tigris River catchment highlighting the litho-structural influence on the fluvial dynamic

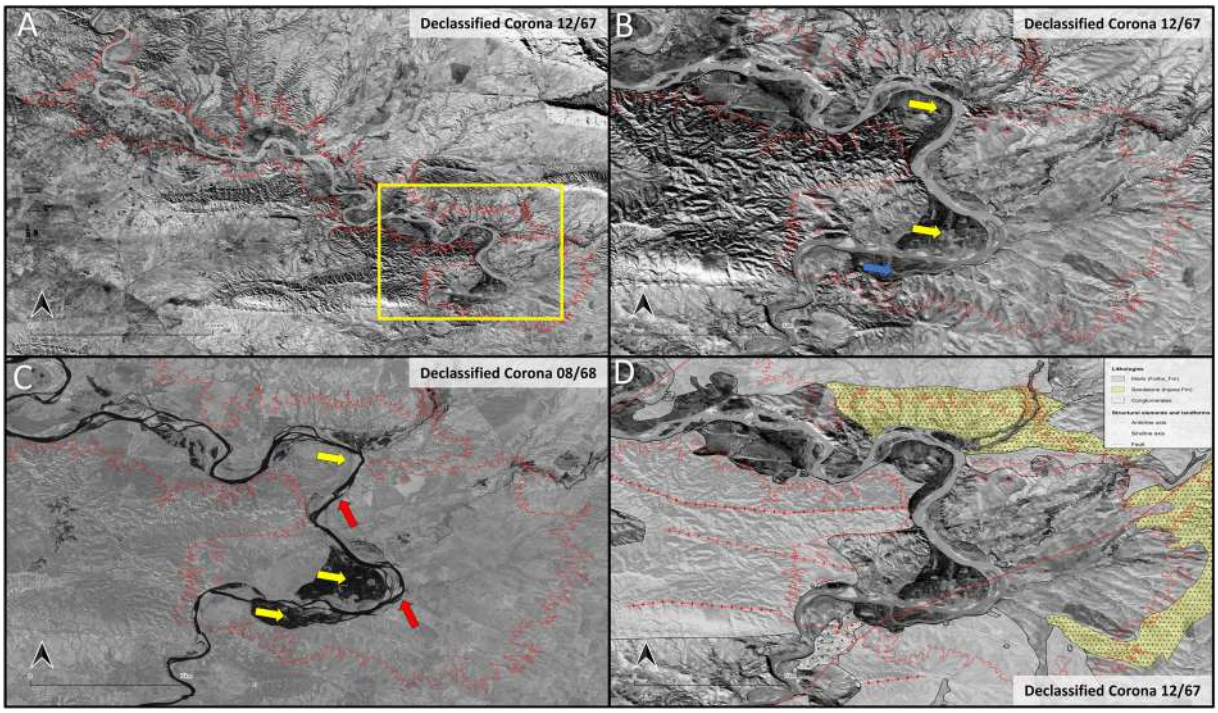


**FIGURE 11** Details from the downstream sector of the river. (A) Position of the area along the Tigris River. Examples from the (B) winter and (C) summer season of the Tigris riverbed. In this portion the river shows a tortuous planform with wide floodplains in the inner bend (yellow arrows). At the low-flow stage, lateral bars and compound bars with point bars are exposed (red arrows). The floodplain located before the dam site is crossed by small secondary branches of the Tigris (blue arrow). Lithological and structural map of this part of the Tigris River catchment highlighting the influence of the anticline/syncline system and lithology on the fluvial dynamic

geomorphological features. Two examples from the upstream portion help in explaining how the Tigris channel belt adjusted to seasonal discharge fluctuations.

In the first example, the Tigris River flows in a partly confined valley, forming a meandering planform; this area is characterized by floodplains and neck cutoffs. In the low-flow stage, the meanders are partly interconnected and filled by water (Figure 12a). During the bankfull stage, a large meander is instead connected to the main Tigris River channel, with the formation of an island covered by vegetation and crossed by a flood channel network (Figure 12b).

The second example shows the effect of the switch in planform geometry caused by the transition from a fine to a coarse-grained channel bedload. There, the seasonal change from bankfull to low-flow stage triggered the shift of many channels from wandering to anabranching (Figures 12c and d).

### 4.5 | The filling of the Mosul Dam Reservoir (1984–1986)

The filling phases of the Mosul Dam Reservoir are reconstructed through the comparison of a selection of Landsat images acquired from 1984 to 1986. Such reconstruction reveals the first impact of the barrage operations on the Tigris River. In 1984 and 1985, the Tigris River was progressively dammed, with an embankment made of a core of silt and clay (Figures 13a–d). At this stage, the shape of the incipient lake in the first area subjected to inundation followed the inherited fluvial landform and valley setting of Tigris River. According to our analysis, the first inundated zones (inundation occurred between the end of 1985 and the beginning of 1986) were the lowlands and the floodplain located near the Mosul Dam site due to the laterally unconfined setting (Figure 13e). Subsequently, upstream migration flooding affected the middle and upstream area, in the meandering and floodplain locations towards the northwest in partly confined and unconfined valley settings (Figures 13f and g). The final filling of the reservoir took 1 year, between June 1985 and July 1986 (Figures 13h and i). The impact on the 1986 annual discharge was important: it was estimated as only 269.88 $m^3/s$, against 546.00 $m^3/s$ for 1984, 624.57 $m^3/s$ for 1985 and 877.93 $m^3/s$ for 1987 (Saleh, 2010).

The impact of the extremely rapid filling phases of the MDL was not confined to the Tigris riverscape; this event also triggered several changes in the local morpho-structural setting around the dam site and the surrounding area. In fact, an increase in local seismic activity was recorded as a swarm of micro-earthquakes between 1986 and 1987; Al-Saigh (2008) suggests that micro-earthquakes were triggered by the large volume of water in the reservoir.

The construction of the dam also affected the aquifers hosted in the bedrock of the dam site, increasing the circulation of groundwater in strata of gypsum with breccias (Fatha Formation). As a result, the rate of karst dissolution of the bedrock increased dramatically. In fact, monitoring surveys of the area after 1985–1986 revealed the development of sinkholes and dolines in proximity of the dam, which also affected the stability of the dam itself (Al-Dabbagh & Al-Naqib, 2009; Al-Saigh, 2008; Kelley et al., 2007).

## 5 | DISCUSSION

### 5.1 | Variations of the Tigris planform and litho-structural control

The mapping of the seasonal riverscape of the Tigris River obtained from the analysis of winter and summer Corona images allows us to reconstruct the behaviour of a part of the river today submerged

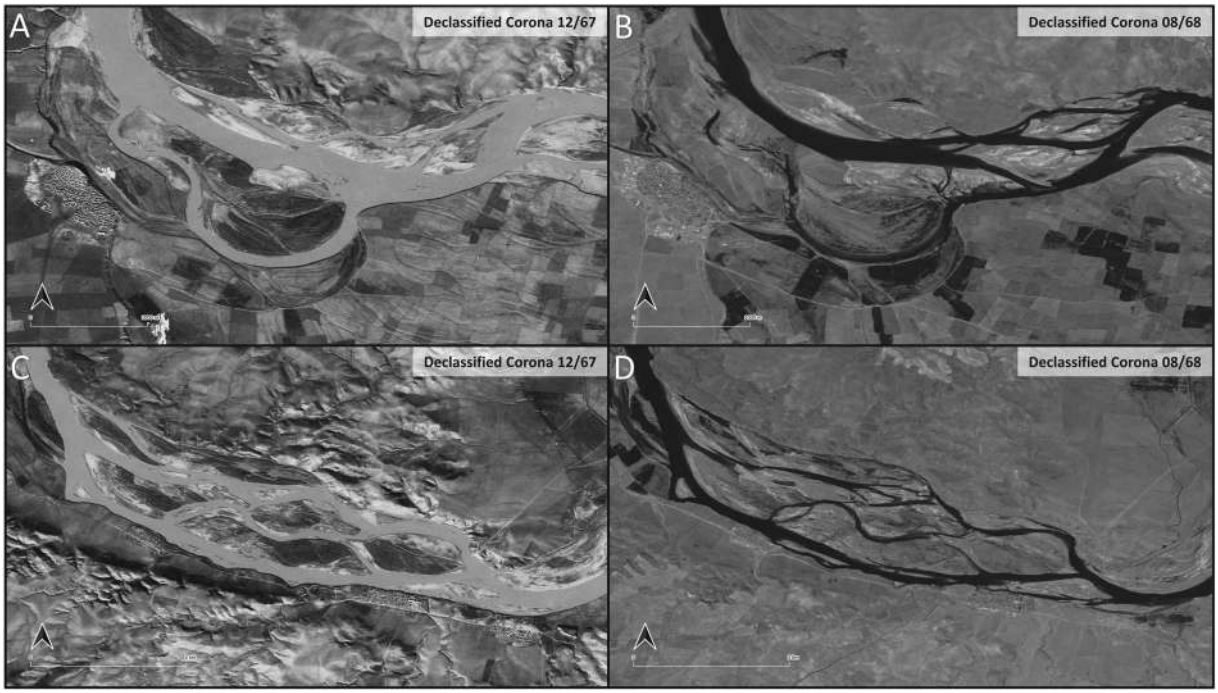


**FIGURE 12** Comparison between the high and low stages of the Tigris River. (A) Large meander connected to main Tigris River channel during the bankfull stage with the formation of an island covered by vegetation and crossed by a flood-channel network. (B) In the same position as (A), meandering planform with floodplains and neck cutoff partly interconnected and filled by water during the low-flow stage. (C) Wandering to (D) anabranching seasonal shift of the fluvial planform from the bankfull to the low-flow stage

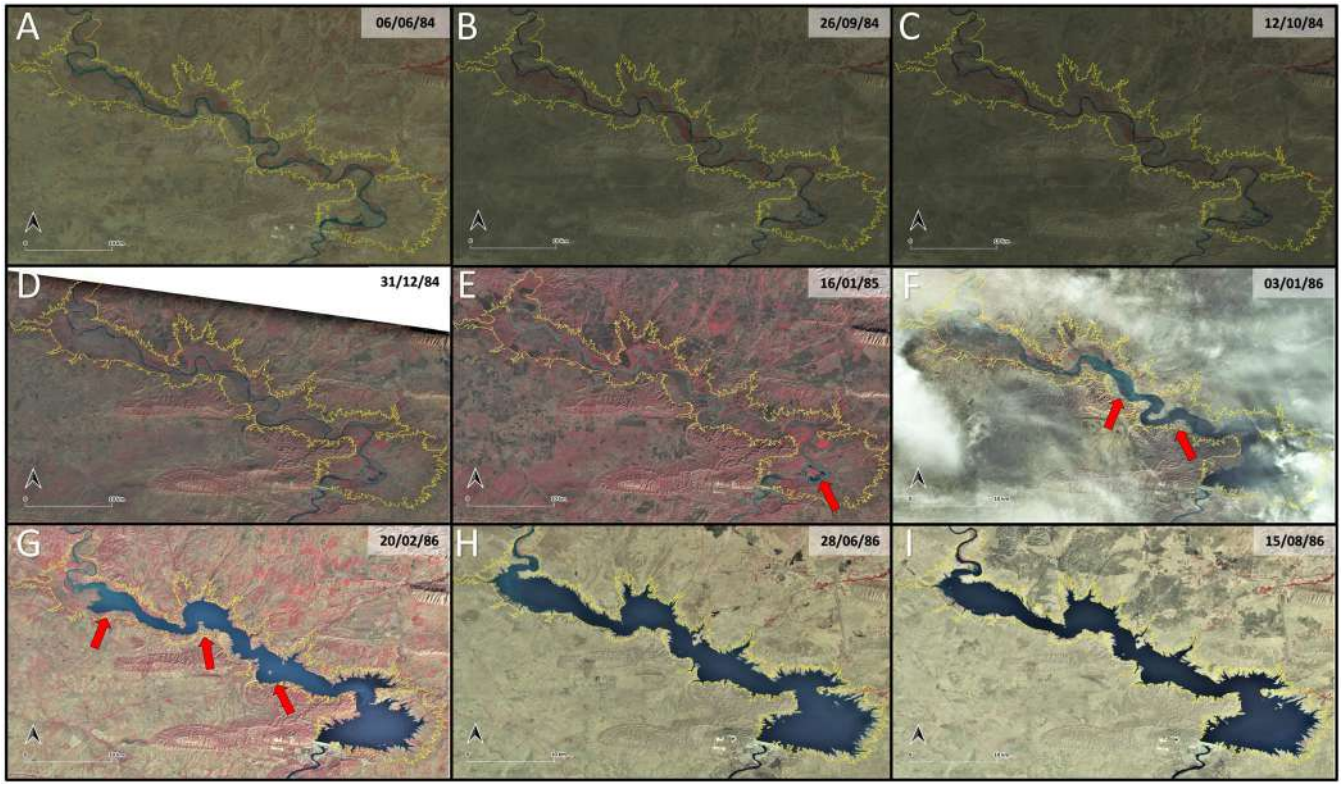


**FIGURE 13** Landsat imagery (false colours) acquired during the filling phases of MDL; the yellow line is the present-day mean lake level. (A–D) Gradual embankment of the Tigris River from June to December 1984. (E) Initial inundation along the lateral unconfined setting near the dam site (red arrows). (F, G) Progressive upstream migration of the flooding, showing the inundation of the meandering area and the floodplain in the partly laterally confined valley (red arrows). (H, I) Final stages of filling of the MDL in the summer of 1986; the basin shape corresponds to the current one

below the MDL. Our results highlight the litho-structural control over the fluvial pattern and the ability of the river to adjust its course during the low and high-flow stages. Seasonal variations of the river discharge switched the processes of sedimentation and erosion, continuously reworking geomorphological features such as middle and point bars. Our observations suggest that local lithology and tectonic settings are the major factors influencing fluvial dynamics, especially for valley setting, slope evolution, sedimentary budget and the general flow direction of the Tigris River (Figure 14a).

Upstream to downstream, it is possible to observe how the Tigris plan morphology changes according to the constraints imposed by these factors. The upstream area shows a meandering pattern, with tortuous meanders switching from wandering (low-flow stage) to anabranching (high-flow stage) (Figures 12c and d); this pattern corresponds to areas with a bedrock composed mainly of marls and conglomerates (Figure 9d). The river behaviour influences the distribution and organization of bars downstream, with the formation of small point and middle bars, and of a gravel bed with transversal bars and plant-covered islands.

Further downstream, the shape and flow direction of the middle and downstream portions are driven by the structure of anticline ridges and the activity of the Dohuk Fault System. Here, the direction and fluvial plan geometry of four distinct reaches clearly follow the strike direction of the anticlines and the Dohuk Fault System (Figure 14b). In the first portion, the Tigris River follows the general direction of the Ain Zala anticline (Figure 14c); here the position of faults controls the downstream increase in sinuosity of the channel to the development of a tortuous meandering course with point bars (Figure 14d). Afterwards, the occurrence of the Ravan anticline triggers a river planform response, changing into an irregular straight planform with lateral bars; here the Tigris River generally flows parallel to the anticline ridge (Figure 14e). Before the dam, in the downstream portion of the river, the impact of the syncline and of the Dohuk Fault System on the shape, flow direction and geomorphic dynamics of the Tigris is more evident. When the river reaches the subsidence area related to the syncline, the degree of sinuosity increases. Also, two meanders, a wide floodplain and fluvial bars in different discharge settings appear (Figure 14f). In the area closest to the dam, the presence of the fault system drives a decrease in sinuosity and a change in the direction of the Tigris flow, that shifts from NW–SE to NE–SW.

## 5.2 | Control of the ancient Tigris riverscape over the shape of the MDL

The actual shape of the Mosul Dam Reservoir is the result of the interplay between the ancient Tigris riverscape, the litho-structural setting of the area and the dam post-filling operations (Figures 2a and b).

During filling operations, the MDL shoreline varies especially between March and July (Khattab et al., 2017; Khattab & Merkel, 2014; Leabi et al., 2020). Sentinel-2 images in March and July 2016 and 2020 record these variations of lake shorelines, especially in the upstream and downstream portions of the newly formed lake

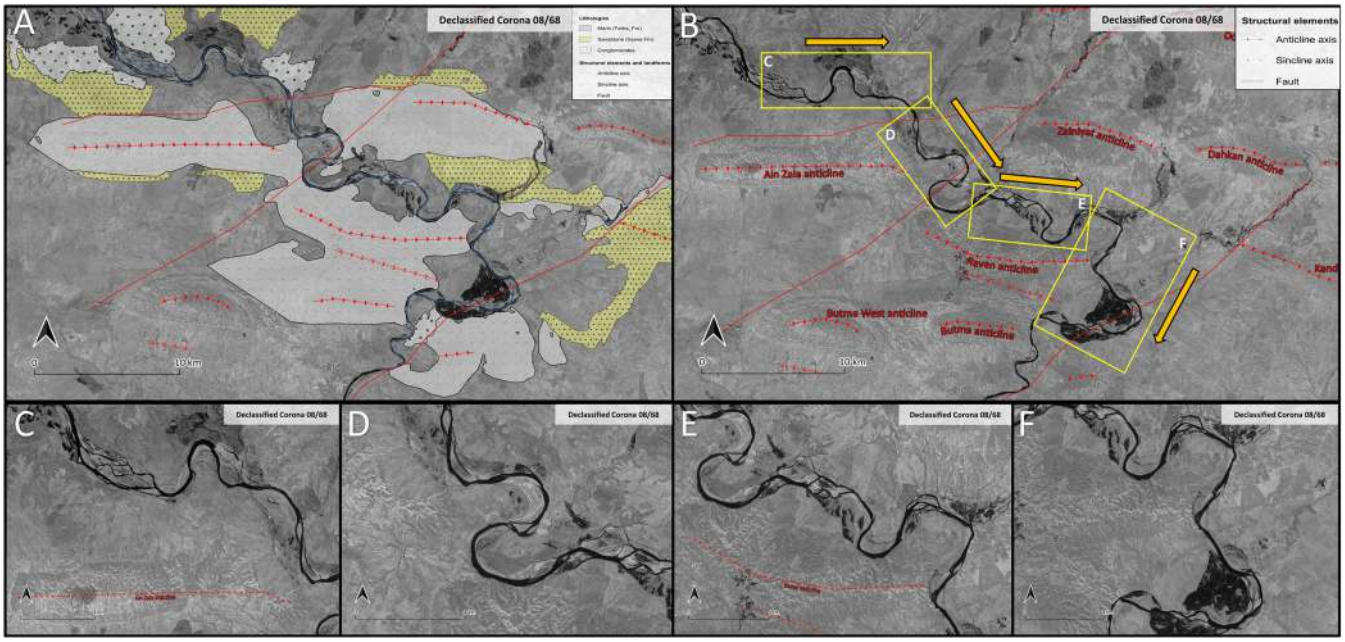


**FIGURE 14** (A) Structural and lithological setting of the study area. (B) Division of the Tigris River into four sections corresponding to main planform and flow direction shifts. (C) Particular of the Tigris flowing W–E parallel to the strike direction of the Ain Zala anticline. (D) Tortuous meanders and NW–SE shifting of the Tigris River. (E) Subsequent changes towards W–E following the growth of the Ravan anticline. (F) Irregular meandering pattern and direction shift towards NE–SW in the downstream portion of the river, due to the combined influence of the Dohuk Fault System and the syncline subsidence

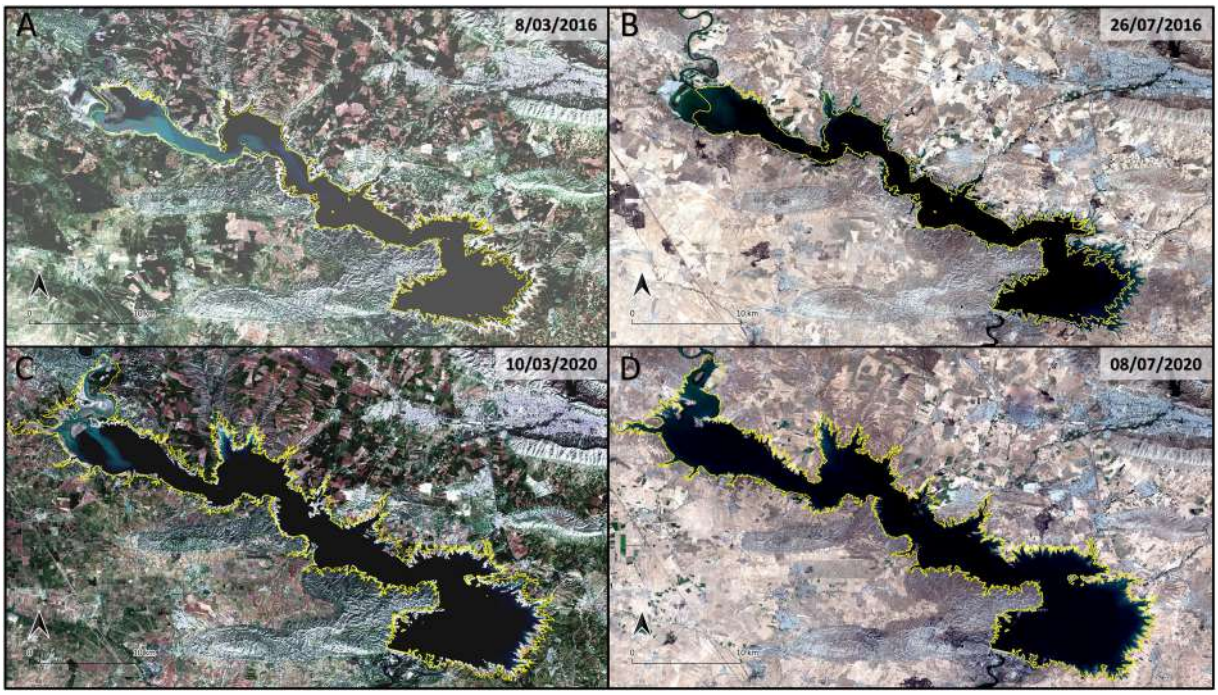


**FIGURE 15** Recent dam operations triggering variations of the MDL water level and its shoreline captured by Sentinel-2 satellite imagery (false colours); lake level variations are also controlled by seasonal changes in fluvial discharge. (A, B) March–July 2016; (C, D) March–July 2020

(Figure 15). Shoreline variations are linked to the seasonal discharge of the Tigris, as evidenced by data from the Ministry of Water Resources of Iraq (Leabi et al., 2020). Dam operations have a relevant impact on the variations of the lake level; for instance, shorelines periodically change in response to the seasonal drop in lake levels, revealing some submerged archaeological sites (Titolo, 2021).

In this scenario, the morphology of the MDL appears to be strongly connected with the ancient geomorphological setting of the Tigris (Figure 16a). The morphology and shoreline of the northern area (upstream) relate to the development of the old meander planform, with the formation of a huge floodplain with neck and chute cutoff processes in a partly unconfined setting. This framework influences

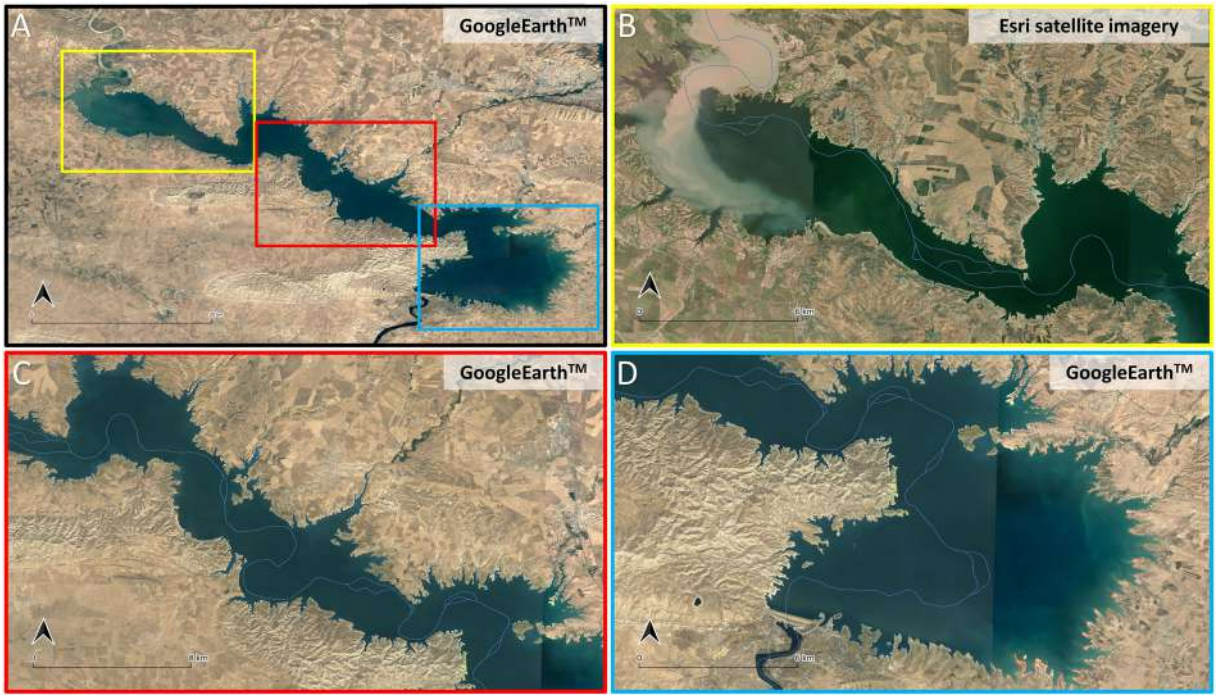


**FIGURE 16** (A) Different portions of the MDL basin as discussed in the text: upstream (yellow box), middle stream (red box) and downstream (blue box); the submerged Tigris River stream is outlined in light blue. (B) The overprint of a submerged meander planform controls the aspect of the basin and shoreline in the upstream portion, also influencing the inlet of the Tigris River into the lake; this is highlighted by the curved shape of the deltaic plume. Afterwards, the narrowing of the lake is controlled by the presence of the confined Tigris River valley (canyon) cut into the Plio-Pleistocene conglomerates, indicating a strong lithological control. (C) The central part of the MDL (middle stream) is characterized by a partly straight, partly arcuate coastline profile on the right banks, influenced by the complex structural setting of the area that alternates faults and folds. (D) At the dam site, the reservoir reaches the maximum surface expansion by occupying the wide flat depression produced by the interplay between the syncline/anticline system and the Dohuk Fault System

the inlet processes of the Tigris, both during flood events and in low-flow stages when a deltaic plain appears (Figure 16b). Afterwards, the narrowing of the lake is due to the same Plio-Pleistocene conglomerate bedrock which turned the course of the Tigris River from a wandering to an anabranching planform, with the formation of plant-covered bars.

The central part of the MDL (middle Tigris River stream) is characterized by a partly straight, partly arcuate coastline profile on the right banks. The complex structural setting of this portion strongly influences the lake shape in the same way as it did with the ancient Tigris River, which displayed a semi-regular meandering planform in a partly confined setting with the development of compound and middle-longitudinal bars. The connections between the ancient Tigris, the structural setting and the present lake morphology are visible in the sub-angular shape of the right banks and in the left tributary derived from the Dohuk Lake and driven by the Dohuk Fault System (Figure 16c).

In the proximity of the dam, the reservoir reaches the maximum surface expansion due to the presence of a wide flat area formed by the interplay between the irregular growth of anticlines and the development of a syncline trough, in which the meandering ancient Tigris River created compound point bars and a floodplain (Figures 2a and 16d).

## CONCLUSIONS

The geomorphological investigation of the submerged riverscape of the Tigris River along the MDL permitted us to reconstruct the dynamic of the river where it is no longer visible, and to identify the main hydrological and geomorphological changes regulated by seasonal variations of the discharge. Moreover, we were also able to correlate the evolution of the Tigris River in response to litho-structural forcing that controlled the size and direction of its course. In fact, variations in the competency of the geological bedrock and the growth of geological structures (faults and folds) resulted in a complex riverscape that—along a relatively short part of the river—alternates between confined and unconfined valleys, straight and meandering courses, anabranching and wandering settings. The same factors have indirect control over the shape of the MDL; in fact, we identify an overprint of the submerged Tigris riverscape on the present-day reservoir that is ultimately related to the major litho-structural forcing factors.

From a more general perspective, our approach confirms the reliability of historical declassified intelligence aerial/satellite pictures in geomorphological studies. In fact, historical remote data, such as the declassified Corona, have a quite high resolution and especially permit us to investigate regions in many cases not accessible and/or where intense urban expansion and human agency have disrupted the natural landforms and altered the pristine surface processes, thus reconstructing the pre-anthropogenic geomorphic dynamic. The case study of the MDL is emblematic because the building of the dam and the infilling of the reservoir completely changed the dynamics of the natural processes and the shrouded pristine landforms. Such an example could help in investigating other regions where less invasive events may have impacted the natural systems, modifying surface processes and the dynamics of the Earth's critical zone. The comparison of present geomorphic settings with historical aerial/satellite

imagery, as much as the use of historical maps, may reveal in detail the impact of the onset of human agency on landscapes in the last few centuries, shedding light on the effect of the Anthropocene on geomorphic surface processes.

## ACKNOWLEDGEMENTS

Field surveys in the region were conducted under the umbrella of the Italian Archaeological Mission to the Kurdistan Region of Iraq of the University of Udine, directed by D. Morandi Bonacossi, who is kindly acknowledged. We are grateful to the General Directorate of Antiquities of the Kurdistan Regional Government, the Directorate of Antiquities of Dohuk and the State Board of Antiquities and Heritage in Baghdad for granting all necessary work permits and their unremitting support. We acknowledge the Editor-in-Chief Professor S.N. Lane for valuable comments and support. Funding for analyses was provided by the Università degli Studi di Milano, Progetto Linea 2 (2017) and Project CTE_NAZPR19AZERB_01 entrusted to A. Zerboni. Part of this research was supported by the Italian Ministry of Education, Universities and Research (MIUR) through the project 'Dipartimenti di Eccellenza 2018–2022' (WP4 – Risorse del Patrimonio Culturale) awarded to the Dipartimento di Scienze della Terra 'A. Desio' of the Università degli Studi di Milano.

## AUTHOR CONTRIBUTIONS

**LF** and **AZ**: Conceptualization, methodology, investigation, writing – original draft preparation, visualization. **GSM**: Methodology, writing – original draft preparation. **FB** and **AP**: Collaboration on data analysis and discussion. All authors approved the final version of the manuscript.

## DATA AVAILABILITY STATEMENT

The datasets used and/or analysed during the current study are available from the corresponding authors on reasonable request.

## ORCID

*Luca Forti* https://orcid.org/0000-0002-2965-9955
*Guido S. Mariani* https://orcid.org/0000-0002-8456-3964
*Filippo Brandolini* https://orcid.org/0000-0001-7970-8578
*Andrea Pezzotta* https://orcid.org/0000-0002-1093-1576
*Andrea Zerboni* https://orcid.org/0000-0002-6844-8528

## REFERENCES

Abdulnaby, W. (2019) Structural geology and neotectonics of Iraq, northwest Zagros. In: Saein, A.Z. (Ed.) *Developments in Structural Geology and Tectonics*, Vol. 3. Amsterdam: Elsevier, pp. 53–73. https://doi.org/10.1016/B978-0-12-815048-1.00004-4

Adamo, N. & Al-Ansari, N. (2016) Mosul dam full story: Safety evaluations of Mosul dam. *Journal of Earth Sciences and Geotechnical Engineering*, 6(3), 185–212. http://urn.kb.se/resolve?urn=urn:nbn:se:ltu:diva-15334

Adamo, N., Al-Ansari, N., Issa, I., Sissakian, V. & Knutsson, S. (2015) Mystery of Mosul Dam the most dangerous dam in the world: Maintenance grouting. *Journal of Earth Sciences and Geotechnical Engineering*, 5(3), 71–77. http://urn.kb.se/resolve?urn=urn:nbn:se:ltu:diva-9410

Adamo, N., Al-Ansari, N., Sissakian, V., Laue, J. & Knutsson, S. (2019) Mosul Dam: Geology and safety concerns. *Journal of Civil Engineering and Architecture*, 13(3), 151–177. Available from: https://doi.org/10.17265/1934-7359/2019.03.001

Al-Ansari, N.A. (2013) Management of water resources in Iraq. *Perspectives and Prognoses: Engineering*, 5(08), 667–668. Available from: https://doi.org/10.4236/eng.2013.58080

Al-Ansari, N.A. & Knutsson, S. (2011) Toward prudent management of water resources in Iraq. *Journal of Advanced Science and Engineering Research*, 1, 53–67. http://urn.kb.se/resolve?urn=urn:nbn:se:ltu:diva-11050

Al-Dabbagh, T.H. & Al-Naqib, S.Q. (1991) Tigris River terrace mapping in northern Iraq and the geotechnical properties of the youngest stage near Dao Al-Qamar village. *Geological Society of London, Special Publications*, 7(1), 603–609. Available from: https://doi.org/10.1144/GSL.ENG.1991.007.01.59

Al-Dabbagh, T.H. & Al-Naqib, S.Q. (2009) The impact of some geologic structural elements on fuse plug south-eastern alignment of Mosul Dam. *Iraq Journal of Earth Science*, 9(2), 27–38.

Al-Khafaji, M.S. & Al-Ameri, R.A. (2021) Evaluation of drought indices correlation for drought frequency analysis of the Mosul dam watershed. *IOP Conference Series: Earth and Environmental Science*, 779(1), 012077. Available from: https://doi.org/10.1088/1755-1315/779/1/012077

Al-Saigh, N. (2008) Seismicity of Mosul dam reservoir. *Iraqi National Journal of Earth Sciences*, 8(2), 11–16. Available from: https://doi.org/10.33899/earth.2008.5481

Al-Saigh, N. (2012) Seismicity of Mosul Dam Reservoir for the monitoring year 1990. *Iraqi National Journal of Earth Sciences*, 12(1), 17–22. Available from: https://doi.org/10.33899/earth.2012.36078

Altinbilek, D. (2004) Development and management of the Euphrates–Tigris basin. *International Journal of Water Resources Development*, 20(1), 15–33. Available from: https://doi.org/10.1080/07900620310001635584

Alwan, I.A., Karim, H.H. & Aziz, N.A. (2019) Agro-climatic zones (ACZ) using climate satellite data in Iraq republic. *IOP Conference Series: Materials Science and Engineering*, 518(2), 022034. https://doi.org/10.1088/1757-899X/518/2/022034

Awchi, T.A. & Kalyana, M.M. (2017) Meteorological drought analysis in northern Iraq using SPI and GIS. *Sustainable Water Resources Management*, 3(4), 451–463. Available from: https://doi.org/10.1007/s40899-017-0111-x

Bing Maps. (2021) *Bing Maps*. Available at: https://www.bing.com/maps (accessed 5 November 2021).

Brierley, G.J. & Fryirs, K.A. (2013) *Geomorphology and River Management: Applications of the River Styles Framework*. Chichester: Wiley.

Brown, A.G., Tooth, S., Bullard, J.E., Thomas, D.S., Chiverrell, R.C., Plater, A.J., Murton, J., Thorndycraft, V.R., Tarolli, P., Rose, J., Wainwright, J., Downs, P. & Aalto, R. (2017) The geomorphology of the Anthropocene: Emergence, status and implications. *Earth Surface Processes and Landforms*, 42(1), 71–90. Available from: https://doi.org/10.1002/esp.394

Buffington, J.M., & Montgomery, D.R. (2013) Geomorphic classification of rivers. In: Shroder, J., & Wohl, E. (Eds.) *Treatise on Geomorphology*. Fluvial Geomorphology, Vol. 9. San Diego, CA: Academic Press, pp. 730–767.

Charlton, R. (2007) *Fundamentals of Fluvial Geomorphology*. Abingdon: Routledge.

Csontos, L., Sasvári, Á., Pocsai, T., Kósa, L., Salae, A.T. & Ali, A. (2012) Structural evolution of the northwestern Zagros, Kurdistan region, Iraq: Implications on oil migration. *GeoArabia*, 17(2), 81–116. Available from: https://doi.org/10.2113/geoarabia170281

Dercourt, J., Zonenshain, L.P., Ricou, L.E., Kazmin, V.G., Le Pichon, X., Knipper, A.L., Grandjacquet, C., Sbortshikov, I.M., Geyssant, J., Lepvrier, C., Pechersky, D.H., Boulin, J., Sibuet, J.C., Savostin, L.A., Sorokhtin, O., Westphal, M. & Bazhenov, M.L. (1986) Geological evolution of the Tethys belt from the Atlantic to the Pamirs since the LIAS. *Tectonophysics*, 123(1–4), 241–315. Available from: https://doi.org/10.1016/0040-1951(86)90199

Dollar, E.S.J. (2004) Fluvial geomorphology. *Progress in Physical Geography: Earth and Environment*, 28(3), 405–450. Available from: https://doi.org/10.1191/0309133304pp419pr

ESCWA. (2013) *Inventory of Shared Water Resources in Western Asia*. Beirut: Salim Dabbous Printing Co.

ESRI. (2021) *World Imagery* [basemap]. Available at: http://www.arcgis.com/home/item.html?id=10df2279f9684e4a9f6a7f08febac2a9 (accessed 11 November 2021).

Forti, L., Perego, A., Brandolini, F., Mariani, G.S., Zebari, M., Nicoll, K., Regattieri, E., Conati, B.C., Morandi Bonacossi, D., Qasim, H.A., Cremaschi, M. & Zerboni, A. (2021) Geomorphology of the northwestern Kurdistan region of Iraq: Landscapes of the Zagros Mountains drained by the Tigris and Great Zab Rivers. *Journal of Maps*, 17(2), 225–236. Available from: https://doi.org/10.1080/17445647.2021.1906339

Fouad, S.F. (2007) Tectonic and structural evolution. *Iraqi Journal of Geology and Mining*, SI 1, 29–50.

Fouad, S.F. (2012) *Tectonic Map of Iraq, Scale 1:1 000 000*, 3rd edition. Baghdad: Iraq Geological Survey Publications.

Gilvear, D. & Bryant, R. (2016) Analysis of remotely sensed data for fluvial geomorphology and river science. In: Kondolf, G.M. & Piégay, H. (Eds.) *Tools in Fluvial Geomorphology*. Chichester: Wiley, pp. 103–132.

Gurnell, A.M., Peiry, J.L. & Petts, G.E. (2003) Using historical data in fluvial geomorphology. In: Kondolf, M. & Piégay, H. (Eds.) *Tools in Fluvial Geomorphology*. Chichester: Wiley, pp. 77–101.

Hasan, M., Moody, A., Benninger, L. & Hedlund, H. (2019) How war, drought, and dam management impact water supply in the Tigris and Euphrates Rivers. *Ambio*, 48(3), 264–279. Available from: https://doi.org/10.1007/s13280-018-1073-4

Jassim, S.Z. & Goff, J.C. (2006) *The Geology of Iraq*. Prague: Dolin.

Jézéquel, C., Oberdorff, T., Tedesco, P.A., & Schmitt, L. (2022) Geomorphological diversity of rivers in the Amazon Basin. *Geomorphology*, 400, 108078.

Kelley, J.R., Wakeley, L.D., Broadfoot, S.W., Pearson, M.L., McGrath, C.J., McGill, T.E., Jorgeson, J.D. & Talbot, C.A. (2007) *Geologic Setting of Mosul Dam and its Engineering Implications*. Vicksburg, MS: USACE-Engineer and Development Center.

Khattab, M.F., Abo, R.K., Al-Muqdadi, S.W. & Merkel, B.J. (2017) Generate reservoir depths mapping by using digital elevation model: A case study of Mosul dam lake, Northern Iraq. *Advances in Remote Sensing*, 6(3), 161–174. Available from: https://doi.org/10.4236/ars.2017.63012

Khattab, M.F. & Merkel, B.J. (2014) Application of Landsat 5 and Landsat 7 images data for water quality mapping in Mosul Dam Lake, Northern Iraq. *Arabian Journal of Geosciences*, 7(9), 3557–3573. Available from: https://doi.org/10.1007/s12517-013-1026-y

Koppen, W. & Geiger, G. (1936) *Das geographisca System der Klimate: Handbuch der Klimatologie*. Borntraeger: Gebr, pp. 1–44.

Leabi, W.K., Wanas, A.H., Nussrat, T.H., Santiago, L.M., Shukri, Z.A. & AbdulKareem, W.S. (2020) Analysis of water flow during the drought and flood seasons case study: The Mosul Dam, Iraq. *IOP Conference Series: Materials Science and Engineering*, 870, 012108. Available from: https://doi.org/10.1088/1757-899X/870/1/012108

Malinowski, J.C. (2002) *Iraq: A Geography*. West Point, NY: United States Military Academy, West Point Department of Geography & Environmental Engineering.

Mouthereau, F., Lacombe, O. & Vergés, J. (2012) Building the Zagros collisional orogen: Timing, strain distribution and the dynamics of Arabia/Eurasia plate convergence. *Tectonophysics*, 532–535, 27–60. Available from: https://doi.org/10.1016/j.tecto.2012.01.022

Othman, A.A. & Gloaguen, R. (2013) River courses affected by landslides and implications for hazard assessment: A high resolution remote sensing case study in NE Iraq–W Iran. *Remote Sensing*, 5(3), 1024–1044. Available from: https://doi.org/10.3390/rs5031024

Perego, A., Zerboni, A. & Cremaschi, M. (2011) Geomorphological map of the Messak Settafet and Mellet (central Sahara, SW Libya). *Journal of Maps*, 7(1), 464–475. Available from: https://doi.org/10.4113/jom.2011.1207

Saleh, D.K. (2010) *Stream Gage Descriptions and Streamflow Statistics for Sites in the Tigris River and Euphrates River Basins, Iraq*. Reston, VA: US Geological Survey.

Salman, S.A., Shahid, S., Ismail, T., Ahmed, K., Chung, E.S. & Wang, X.J. (2019) Characteristics of annual and seasonal trends of rainfall and temperature in Iraq. *Asia-Pacific Journal of Atmospheric Sciences*, 55(3), 429–438. Available from: https://doi.org/10.1007/s13143-018-0073-4

Sconzo, P. & Simi, F. (2020) Settlement dynamics on the banks of the Upper Tigris, Iraq: The Mosul Dam Reservoir Survey (1980). *Journal of Open Archaeology Data*, 8(1), 3. Available from: https://doi.org/10.5334/joad.63

Sissakian, V., Al-Ansari, N. & Knutsson, S. (2014) Karstification effect on the stability of Mosul Dam and its assessment, North Iraq. *Engineering*, 6(2), 84–92. Available from: https://doi.org/10.4236/eng.2014.62012

Sissakian, V.K., Adamo, N. & Al-Ansari, N. (2020) The role of geological investigations for dam siting: Mosul Dam a case study. *Geotechnical and Geological Engineering*, 38(2), 2085–2096. Available from: https://doi.org/10.1007/s10706-019-01150-2

Sissakian, V.K., Adamo, N., Al-Ansari, N., Knutsson, S., Laue, J. & Elagely, M. (2018) A comparative study of Mosul and Haditha dams, Iraq: Geological conditions. *Journal of Earth Sciences and Geotechnical Engineering*, 8(2), 35–52. http://urn.kb.se/resolve?urn=urn:nbn:se:ltu:diva-67809

Sissakian, V.K. & Al-Jibouri, B.S. (2012) Stratigraphy of the low folded zone. *Iraqi Bulletin of Geology and Mining*, 5, 63–132.

Sissakian, V.K. & Fouad, S.F. (2012) *Geological Map of Iraq, Scale 1: 1 000 000*, 4th edition. Baghdad: Iraq Geological Survey Publications.

Sulaiman, A.H. (2016) Development of probability diagram for an observed annual rainfall in (Duhok and Sartang-Summel) Iraqi Kurdistan. In *Proceedings of the 2nd Scientific Agricultural Conference, 26-27 April 2016, Duhok*.

Tadaki, M., Brierley, G., & Cullum, C. (2014) River classification: theory, practice, politics. *Wiley Interdisciplinary Reviews: Water*, 1(4), 349–367.

Tarolli, P., Cao, W., Sofia, G., Evans, D. & Ellis, E.C. (2019) From features to fingerprints: A general diagnostic framework for anthropogenic geomorphology. *Progress in Physical Geography: Earth and Environment*, 43(1), 95–128. Available from: https://doi.org/10.1177/0309133318825284

Thorndycraft, V.R., Benito, G. & Gregory, K.J. (2008) Fluvial geomorphology: A perspective on current status and methods. *Geomorphology*, 98(1–2), 2–12. Available from: https://doi.org/10.1016/j.geomorph.2007.02.023

Titolo, A. (2021) Use of time-series NDWI to monitor emerging archaeological sites: Case studies from Iraqi artificial reservoirs. *Remote Sensing*, 13(4), 786. Available from: https://doi.org/10.3390/rs13040786

USGS. (1968) *Declassified Corona imaging data*. Available at: https://corona.cast.uark.edu (accessed 11 August 2020).

Yamazaki, D., Ikeshima, D., Tawatari, R., Yamaguchi, T., O'Loughlin, F., Neal, J.C., Sampson, C.C., Kanae, S. & Bates, P.D. (2017) A high accuracy map of global terrain elevations. *Geophysical Research Letters*, 44(11), 5844–5853. Available from: https://doi.org/10.1002/2017GL072874

Zerboni, A., Brandolini, F., Mariani, G.S., Perego, A., Salvatori, S., Usai, D., Pelfini, M. & Williams, M.A.J. (2020) The Khartoum–Omdurman conurbation: A growing megacity at the confluence of the Blue and White Nile Rivers. *Journal of Maps*, 17(4), 227–240. Available from: https://doi.org/10.1080/17445647.2020.1758810

**How to cite this article:** Forti, L., Mariani, G.S., Brandolini, F., Pezzotta, A. & Zerboni, A. (2022) Declassified intelligence satellite imagery as a tool to reconstruct past landforms and surface processes: The submerged riverscape of the Tigris River below the Mosul Dam Lake, Iraq. *Earth Surface Processes and Landforms*, 1–17. Available from: https://doi.org/10.1002/esp.5389